Published in final edited form as:
Free Radic Biol Med. 2008 October 1; 45(7): 943–949. doi:10.1016/j.freeradbiomed.2008.05.015.

Pharmacokinetics of the potent redox modulating manganese porphyrin, MnTE-2-PyP^{5+} in plasma and major organs of B6C3F1 mice

Ivan Spasojević[1*], **Yumin Chen**[2], **Teresa J. Noel**[2], **Ping Fan**[1], **Lichun Zhang**[1], **Julio S. Rebouças**[3], **Daret K. St. Clair**[2], and **Ines Batinić-Haberle**[3*]

1*Department of Medicine, Duke University Medical School, Durham, NC 27710*

2*Graduate Center for Toxicology, University of Kentucky, Lexington, KY, 40536*

3*Department of Radiation Oncology, Duke University Medical School, Durham, NC 27710*

Abstract

Mn(III)tetrakis(*N*-ethylpyridinium-2-yl)porphyrin, MnTE-2-PyP^{5+}, a potent catalytic superoxide and peroxynitrite scavenger, has been beneficial in several oxidative stress-related disease thus far examined. Pharmacokinetic studies are essential for the better assessment of the therapeutic potential of MnTE-2-PyP^{5+} and similar compounds, as well as for the modulation of their bioavailability and toxicity. Despite high hydrophilicity, this drug entered mitochondria after single 10 mg/kg intraperitoneal injection at levels high enough (5.1 μM; 2.95 ng/mg protein) to protect it against superoxide/peroxynitrite damage. Utilizing the same analytical approach, which involves the reduction of MnTE-2-PyP^{5+}, followed by the exchange of Mn^{2+} with Zn^{2+}, and HPLC/fluorescence detection of ZnTE-2-PyP^{4+}, we measured levels of MnTE-2-PyP^{5+} in mouse plasma, liver, kidney, lung, heart, spleen, and brain over a period of 7 days after a single intraperitoneal injection of 10 mg/kg. Two B6C3F1 female mice per time point were used. The pharmacokinetic profile in plasma and organs was complex; thus a non-compartmental approach was utilized to calculate the area under the curve (AUC), c_{max}, t_{max}, and drug elimination half-time ($t_{1/2}$). In terms of levels of MnTE-2-PyP^{5+} found, the organs can be classified into 3 distinct groups: (1) high levels: kidney, liver, and spleen; (2) moderate levels: lung and heart; and (3) low levels: brain. The maximal levels in plasma, kidney, spleen, lung, and heart are reached within first 45 minutes whereas in case of liver a prolonged absorption phase was observed with the maximal concentration reached at 8 hours. Moreover, accumulation of the drug in brain continues beyond time of the experiment (7 days) and is likely driven by the presence of negatively charged phospholipids. For tissues other than brain, a slow elimination phase (single exponential decay, $t_{1/2}$ = 60 to 135 hours) is observed. The calculated pharmacokinetic parameters will be used to design optimal dosing regimens in future preclinical studies utilizing this and similar compounds.

*Corresponding authors: **Ivan Spasojević** Department of Medicine, Duke University Medical Center, Durham, NC 27710, Tel: 684-8311, Fax: 684-9094, e-mail: spaso001@mc.duke.edu, **Ines Batinić-Haberle**, Department of Radiation Oncology, Duke University Medical Center, 231 Nanaline H. Duke, Box 3711, Durham, NC 27710, Tel: 919-684-2101, Fax: 919-684-8885, e-mail: iBatinić@duke.edu.

Keywords

MnTE-2-PyP^{5+}; AEOL 10113; SOD mimic; pharmacokinetics in mouse plasma; pharmacokinetics in mouse organs; pharmacokinetics in mouse tissues

Introduction

For more than a decade we have been investigating metalloporphyrin-based antioxidants, studying their *in vitro* efficacy in eliminating reactive species and *in vivo* efficacy in oxidative stress-related models of diseases [1–8]. From our studies on structure-activity relationships between the redox potential of metalloporphyrins and their ability to dismute superoxide, $O_2^{\cdot -}$, MnTE-2-PyP^{5+} emerged as a standard potent catalytic antioxidant now used a wide range of cellular and animal studies. The compound has a high efficacy to *dismute (disproportionate)* O_2^- [1,2] (log k_{cat} =7.76 as compared to log k_{cat} = 8.84 - 9.3 for SOD enzymes [9–14]). Moreover, its efficacy to dismute $O_2^{\cdot -}$ parallels its efficacy to *reduce* peroxynitrite, $ONOO^-$, (log k_{red} = 7.53) [15,16]. MnTE-2-PyP^{5+} is also very effective in scavenging carbonate radical, $CO_3^{\cdot -}$ [16]. The reduction of peroxynitrite or $CO_3^{\cdot -}$ is catalytic in nature *in vivo*, as it is coupled to cellular reductants; the overall reaction is more efficient with ascorbate, and urate than with potential targets such as thiols and amino acids [15–17]. The ability to eliminate $O_2^{\cdot -}$, $ONOO^-$, and $CO_{3.-}$ exceeds that of other compounds presently in preclinical and clinical studies such as Mn salen derivatives [18,19], Mn cyclic polyamines [20], nitrones [21,22], nitroxides [23], MitoQ [24] and analogous compounds [25]. MnTE-2-PyP^{5+} ameliorates oxidative stress-related diseases, presumably through elimination of reactive species, thus providing the protection of most biologically relevant targets against *primary oxidative stress*. Moreover, the elimination of reactive species prevents activation of transcription factors AP-1 [26,27], HIF-1α [28–31], and NF-κB [32,33] which in turn inhibits the expression of cytokines and/or enzymes that would otherwise perpetuate *secondary oxidative stress*. The catalytic power of MnTE-2-PyP^{5+} is enhanced by the presence of electron-withdrawing positively charged *ortho* alkylpyridyl groups close to the metal center. These proximal positive charges contribute to both *thermodynamic* (favorable redox potential) [1,6] and *kinetic* (electrostatic attraction of the negatively charged substrate) [6,34] facilitation of $O_2^{\cdot -}$ dismutation, and $ONOO^-$ and $CO_3^{\cdot -}$ reduction. Several other metalloporphyrins [35−38] and corroles [39] have been developed that exploit the effects of cationic *ortho* quaternary nitrogens.

The beneficial effects of Mn alkylpyridylporphyrins have been observed in central nervous system injuries (stroke [40−42], spinal cord injury [43], ALS [44], Alzhemier's disease [45]), radiation injury [46–49], cancer [26,29], diabetes [50,51], sickle cell disease [52], ischemia/reperfusion conditions [53–55], arthritis [56] and others. However, very little is known about the bioavailability, site of action and pharmacokinetics and toxicology of the compound. It has been assumed in past that excessive hydrophilicity would limit the accumulation of MnTE-2-PyP^{5+} within the cell and its organelles, suggesting the *extracellular* localization of porphyrin as a likely site of action. However, the high efficacy observed *in vivo* strongly implicated not only *cytosol*, but also *mitochondrion* [26,27] and *nucleus* [32,33] as possible sites of action. In order to test the validity of such conclusions we have developed a sensitive HPLC/fluorescence method for determination of the positively charged Mn(III) *ortho N*-alkylpyridylporphyrins *in vivo*, and used it in a mouse mitochondrial study [57]. Herein, utilizing similar analytical approach, we undertook a pharmacokinetic study to detect levels of porphyrin in mouse plasma and different organs over the period of 7 days after single 10 mg/kg intraperitoneal injection of MnTE-2-PyP^{5+}. This is the first detailed pharmacokinetic study on such an important class of Mn-porphyrin-based antioxidant therapeutics.

Experimental

General

Sodium L-ascorbate, mannitol, albumin from bovine serum (BSA), and $ZnCl_2$ were from Sigma and $Zn(CH_3COO)_2 \times 2\ H_2O$ from J. T. Baker. Acetonitrile and trifluoroacetic acid (TFA) were from Fisher Scientific and triethylamine from Pierce. Methanol (anhydrous, absolute) was from Mallinckrodt. Glacial acetic acid was from EM Science. Phosphate-buffered saline (50 mM sodium phosphate, 0.9% NaCl, pH 7.4) (PBS) was from Gibco.

Porphyrins

MnTE-2-PyP^{5+} (λ_{max} = 454 nm, log ε = 5.14) [1,2], and ZnTE-2-PyP^{4+} (λ_{max} = 425.5 nm, log ε =5.46) [57–59] were prepared as described previously. ZnTnBu-2-PyP^{4+} was used as an internal standard and was prepared and characterized as described [57].

Uv/vis spectroscopy

Uv/vis was done on a Shimadzu 2501 PC UV/Vis spectrophotometer.

Mice

The University of Kentucky Medical Center Research Animal Facility has a continuously accredited program from AAALAC International. All experiments using animals were performed according to the approved protocol for humanely care and use of animals. Two B6C3F1/J female mice were used for each time point. (This strain is commonly used as a background strain for transgenic MnSOD mice used in studying oxidative stress injuries.) The mice weighted from 20 to 25 g and the volumes of porphyrin saline solutions ranged accordingly from 200 to 250 μL. The mice were euthanatized with high-dose pentobarbital. Before harvesting tissue, the animals were perfused with saline to avoid artifacts related to the retention of blood in the organs and tissue. All mice perfused had their blood drawn from the left ventricle. The perfusion was by gravity flow of saline via a blunt needle placed into the aorta through left ventricle and the saline flow through right atrium was continued until the liver cleared out.

Protein levels

The protein levels were determined in plasma and tissue homogenates by colorimetric Bradford assay as specified by manufacturer (Bio-Rad, Richmond CA). Protein levels were used to normalize tissue levels in homogenates.

MnTE-2-PyP^{5+} plasma/tissue extraction

Organs were cryo-pulverized in a Bessman tissue pulverizer (BioSpec Products, Bartlesville, OK) under liquid nitrogen and then homogenized in rotary homogenizer (PTFE pestle and glass tube) with 2 volumes of deionized water. 100 μL of either plasma or tissue homogenate was transferred into a 2 mL polypropylene screw-cap vial and 200 μL of deionized water and 300 μL of 1% acetic acid in methanol were added. The content was mixed in a multi-vortexer for 60 sec and the homogenate was centrifuged 5 min at 16,000 g. 400 μL of the supernatant was pipetted into a 5 mL polypropylene tube (10 × 50 mm) and the solvent was completely removed in a Savant Speed-Vac evaporator at 40 °C within 1 h. The dry residue was dissolved in 100 μL of deionized water containing 20 mM triethylamine, the pH of which was adjusted with diluted TFA to pH 6.2, followed by 60 sec vortexing and centrifugation for 2 min at 2000 g. 80 μL of the supernatant was transferred into a 2 mL polypropylene screw-cap tube, and 30 μL of 1.0 M either Zn acetate or Zn chloride in water and 10 μL of freshly prepared 0.11 M sodium ascorbate in water were added. The solution was left for one hour at either 50 °C or 70 °C. (If working at 70 °C the more acidic salt Zn chloride ought to be used due to a lower degree

of hydrolysis than that of Zn acetate). 20 μL of 2.7 M TFA and 20 μL of 800 nM ZnTnBu-2-PyP^{4+} were added, followed by vortexing for 60 sec and centrifugation for 5 min at 16,000 g. 110 μL of the supernatant was transferred to the HPLC autosampler polypropylene vial equipped with silicone/PTFE septum.

HPLC

Equipment: Waters 2695 HPLC system (pump, autosampler, column oven) and Waters, model 2475 fluorescence detector set on Gain 100, λ_{exc} = 425 nm and λ_{abs} = 656 nm [60–62]. Column: YMC-Pack, ODS-AM, C18 column (3 μm particle size, 120 Å pore size, 150 × 4.6 mm) at 45 °C. Solvent A: 95% aqueous (deionized water, 20 mM triethylamine, pH 2.7 adjusted with concentrated TFA) and 5% acetonitrile. Solvent B: acetonitrile. Elution gradient at 1.5 mL/min: 0-15-20 min, 100% A - 80% A - 100% A, followed by 5 min column conditioning. Autosampler temperature: 4 °C. Injection volume: 80 μL.

The *ortho* isomers of MnTE-2-PyP^{5+}, ZnTE-2-PyP^{4+} and their parent metal-free ligand, H_2TE-2-PyP^{4+} have atropoisomers, which we previously characterized by HPLC/uv/vis/NMR and X-ray methods [59]. We observed that the abundance ratio of the four isomers of ZnTE-2-PyP^{4+} and their retention times on HPLC were the same in mouse heart mitochondrial homogenates [57], in processed mouse organ homogenates or in aqueous solution [58]. This indicated that the interactions of any of the four atropoisomers with cellular components [57, 58] are not strong enough to overcome the rotational barrier of the alkylpyridyl “arms” which would cause a change in the abundance ratio of atropoisomers. The experiments also implied that the Mn porphyrin does not undergo oxidative degradation or any other modification *in vivo*. Using any of the atropoisomers for calculation of the levels of MnTE-2-PyP^{5+} in mitochondria gave the same result. ZnTnBu-2-PyP^{4+} was used as an internal standard, and its atropoisomers were also present in the chromatogram at the expected abundance ratio [57, 58]. The assignment of the individual atropoisomers, αααα, αααβ, ααββ and αβαβ,of both Zn porphyrins was done based on our previous HPLC/^{1}H NMR/X-ray study [57,58]. In this study, the most abundant atropoisomer, αααβ, was used for the quantification of both ZnTE-2-PyP^{5+} and ZnTnBu-2-PyP^{4+} (internal standard).

Calibration curves

A set of serially diluted standard samples of MnTE-2-PyP^{5+} were prepared for calibration. The range varied from 1.5 ng to 100 μg per mL of drug-free plasma or per g of drug-free wet tissue, and was dependent upon the type of the organ studied. MnTE-2-PyP^{5+} was added into the tissue homogenate or plasma, followed by 15-min incubation at room temperature. The rest of the assay procedure was identical to the procedure performed with organs and plasma of drug-treated animals. Response was calculated as the ratio between standard peak area/internal standard peak area.

Recovery of MnTE-2-PyP^{5+}, i.e. the overall efficacy of extraction from plasma and organs plus Mn-to-Zn exchange, was determined in triplicates in the following way. A known amount of MnTE-2-PyP^{5+} was added to plasma or organ homogenate, and the procedure of extraction/metal exchange was followed. The response from this experiment was compared to the response of the sample where corresponding amount of ZnTE-2-PyP^{4+} (equal to 100% yield of MnTE-2-PyP^{5+}) was diluted into mobile phase. The obtained recovery values are 83% in plasma, 89% in liver, 88% in kidney, 83% in spleen, 70% in lung, 85% in heart, 97% in brain.

Results and Discussion

MnTE-2-PyP^{5+} is very effective in eliminating reactive species (RS), particularly $O_2^{\cdot -}$ and $ONOO^-$, with rate constants that are among the highest when compared to other synthetic

antioxidants [1–8,15–17]. This allows the compound not only to decrease the *primary insult* of RS to biological molecules, but also to inhibit activation of transcription factors which in turn leads to suppression of expression of those cytokines and enzymes that perpetuate *secondary oxidative stress* [26–33]. Thus the MnTE-2-PyP^{5+} has a potential to be an efficacious therapeutic in all diseases that have oxidative stress as a common factor [40–56]. Due to its high hydrophilicity and positive charge, crossing the blood brain barrier and the mitochondrial envelope has always been a concern. Thus, we were surprised to find 5.1 μM (2.95 ng/mg protein) MnTE-2-PyP^{5+} in mouse heart mitochondria 4 (or 7) hours after a single 10 mg/kg intraperintoneal injection; as a note, 10 mg/kg is the most commonly used (as single or multiple) therapeutic dose of this porphyrin [57]. A previous study by Ferrer-Sueta *et al* [17] on submitochondrial particles indicate that at ≥3 μM MnTE-2-PyP^{5+} nearly fully eliminates $ONOO^-$ mediated damage to the components of mitochondrial respiration machinery. The dose of 10 mg/kg was picked up based upon the rodent studies on the diabetes [50], cancer [28,29,63], and radioprotection [48,64] that have reported beneficial effects (delayed onset of diabetes, tumor growth delay, radioprotection) when MnTE-2-PyP^{5+} was administered at doses ranging from 6 to 15 mg/kg. The TD_{50} was found to be 91.5 mg when MnTE-2-PyP^{5+} was administered subcutaneously.[a]

We have reported that Mn porphyrins can mimic cyt P450, yet to a lower extent than Fe analogous porphyrins [65]. It was also shown that Mn porphyrin can redox cycle with cyt P450 reductase which action was claimed to have possible beneficial and/or adverse effects [66]. Thus far our studies did not indicate any metabolism of MnTE-2-PyP^{5+} and similar cationic porphyrins by enzymatic systems *in vivo*.

Herein, we studied the pharmacokinetics (PK) of MnTE-2-PyP^{5+} in mouse plasma and several important organs. Animal perfusion to remove blood from organs, and measurement of porphyrin levels were performed as in mitochondrial study [57] but with some necessary modifications primarily in sample preparation procedures. The HPLC/fluorescence method is based on the reduction of MnTE-2-PyP^{5+} by ascorbic acid, followed by *in situ* Mn^{2+} to Zn^{2+} exchange and fluorescence detection of ZnTE-2-PyP^{4+}. Assay conditions are given in Scheme I. ZnTnBu-2-PyP^{4+} was used as an internal standard. Calibration curves, made with drug-free plasma and corresponding organ homogenates, were linear in the ranges needed for quantification. Lower limits of quantification (LLQ) in ng/mL (plasma) or ng/g wet tissue (organs), with corresponding sample size in brackets, were as follows: plasma 4.64, (100 μL), liver 11.9 (33 mg), spleen 72.5 (33 mg), kidney 215 (33 mg), lung 35.8 (33 mg), heart 35.8 (33 mg), and brain 3.6 (100 mg). Accuracy (relative error) acceptance criteria at each nominal concentration were <15% and <20% at LLQ [67]. The concentration in day 7 plasma samples was barely detectable and outside the standard curve range (below LLQ). Nonetheless, in the course of manuscript preparation, a new LC/MS/MS method for MnTE-2-PyP^{5+} in plasma has been developed in our lab with LLQ = 0.5 ng/mL using 250 μL sample. Thus, the pooled day 7 plasma sample (2 animals) was measured by LC/MS/MS and the method will be described in a subsequent publication.

Pharmacokinetic profiles are shown in Figure 1A–G along with corresponding calibration curves. The levels of porphyrin are given in μg/g wet tissue or μg/mL plasma. For each time-point the two concentrations measured, corresponding to two animals, are presented as open circles whereas the average of these values is given by the solid bold line. Average concentrations at each time point were used in the pharmacokinetic calculations. Semi-log plots are chosen to illustrate the level of complexity in the PK behavior. Namely, a single-exponential rise/decay in concentration would indicate drug absorption/distribution from/into one or more “compartments” of very similar blood perfusion and/or drug affinity properties. Such single-

[a]Panni, M, The TD_{50} of MnTE-2-PyP^{5+} given subcutaneously.

exponential process would appear linear in a semi-log plot. Thus, as it can be seen in Figure 1A (far left), plasma pharmacokinetics over 7 days appears to be very complex –several linear regions (compartments) can be recognized. This is in agreement with the pharmacokinetics seen in different organs (Figures 1B–G). For this reason, and because of limited number of time points, no attempt was made to fit a multi-compartmental model into the data. Instead, the non-compartmental approach (WinNonlin, Pharsight Inc.) was used: numerical integration of the PK profile is performed to calculate the area under the curve (AUC), and the terminal slope is used to calculate drug half-time ($t_{1/2}$) for each organ and plasma; c_{max} is the highest concentration found along the PK profile, and t_{max} is the corresponding time (Table 1). In terms of levels of MnTE-2-PyP^{5+} found, the organs can be classified into 3 distinct groups: (1) high levels: kidney, liver, and spleen; (2) moderate levels: lung and heart; and (3) low levels: brain. The plots clearly reveal differences in the drug penetration (diffusion or active transport), and drug-tissue affinity (binding or retention) among organs. During the first 15 minutes, the drug is rapidly absorbed from the intraperitoneal cavity into the plasma. The levels in kidney, spleen, lung, and heart also increase rapildy, presumably due to a passive diffusion - the drug levels in kidney reach especially high values, obviously due to both high penetration and a high affinity. At the same time, in liver, the drug shows a slow penetration (t_{max} = 8 hrs) but reaching very high levels due to high affinity. The drug also exhibits a very slow penetration into brain. Due to different affinity (weak versus strong) for the different tissues, an intensive distribution/re-distribution of the drug in the body is going on for 2 days after which a slow drug elimination from all organs (except brain) takes place at a similar rate. The MnTE-2-PyP^{5+} levels in brain, however, start *increasing* after 2 days and continue the trend past 7 days meaning that the drug binds very strongly to the brain tissue; it is noteworthy that brain continues to accumulate MnTE-2-PyP^{5+} despite very low and ever decreasing concentration of the drug in circulating blood (plasma) (Figure 1G). This accumulation of the drug in the brain at late times is maintained by the high concentration of MnTE-2-PyP^{5+} in other tissues (liver, kidney, and spleen) from where it is supplied over days and weeks via re-distribution.

We have already found that positively charged isomeric Mn(III) methylpyridylporphyrins (MnTM-2(3,4)-PyP^{5+} associate with the nucleic acids of *E. coli* [1]. Its cationic nature further drives the accumulation of MnTE-2-PyP^{5+} in mitochondria [57]. Finally, a study in collaboration with Tse and Piganelli,[b] showed that MnTE-2-PyP^{5+} accumulates 3-fold more in the nucleus than in the cytosol of macrophages, presumably driven by the negatively charged phosphate groups of the nucleic acids. Similarly, the accumulation of MnTE-2-PyP^{5+} in brain is likely driven by the abundance of negatively charged phospholipids in this organ, and may explain the beneficial effects of MnTE-2-PyP^{5+} in ALS [44], stroke models [41,42] and pain management [68]. Further it is well-documented that overexpression of MnSOD can suppress cancer phenotypes and the metastasic potential of cancer cells; all suggesting a high therapeutic potential of MnTE-2-PyP^{5+} for brain radioprotection and brain tumor treatment.

The ability of MnTE-2-PyP^{5+} to cross blood brain barrier has been indicated in an independent study where nearly full reversal of morphine tolerance was achieved by MnTE-2-PyP^{5+} therapy; moreover, identical effects were observed whether MnTE-2-PyP^{5+} was administered intraperitoneally or intrathecally [63,68]. Further, when *para* methyl analogue, MnTM-4-PyP^{5+} was used in a rabbit model of cerebral palsy its presence in fetal brain was observed by MRI.[c] More thorough study is in progress to evaluate whether brain levels achieved by the intraperitoneal or subcutaneous routes are close to the therapeutic levels in different animal models of central nervous system injuries.

[b] Spasojević, I.; Batinić-Haberle, I.; Tse, H.; Piganelli, J. Accumulation of MnTE-2-PyP^{5+} in nucleus, unpublished

[c] Sidhartha, T. MnTM-4-PyP^{5+} in cerebral palsy, unpublished.

The levels of MnTE-2-PyP^{5+} ≥ 3 μM in submitochondrial particles shown to be protective by Ferrer-Sueta et al [17], coincide with levels at which the aerobic growth SOD-deficient *E. coli* achieves ≥ 60 % of the growth of the wild type [1,69]. Based on Vinnakota and Bassingthwaighte data on the density of myocardial tissue to be 1.053 g/mL [70], and assuming that it is valid for other tissues as well, the 1 μg/g wet tissue is ~1 μM MnTE-2-PyP^{5+} (M_r = 965.13). Consequently, after single intraperitoneal injection, therapeutic doses of MnTE-2-PyP^{5+} might have been achieved in liver, kidney and spleen. This is in agreement with Saba *et al* data [54] where kidney ischemia/reperfusion injury was significantly diminished by a single intravenous injection of hexyl analogue, MnTnHex-2-PyP^{5+}. More studies are needed to determine the magnitude and the frequency of administrations needed to achieve therapeutic doses in other organs.

Conclusions

We report here the first detailed pharmacokinetic study on an important class of catalytic Mn-porphyrin-based antioxidant therapeutics. The findings presented are relevant for the proper dosing of MnTE-2-PyP^{5+} in future *in vivo* studies. The PK analysis shows a very efficient absorption of the drug from intraperitoneal space into blood stream (within 15 min) and a very slow elimination of the drug from the body ($t_{1/2}$ = 55–135 hrs). After single dose, near-therapeutic levels were achieved in liver, kidneys, and spleen. The observed high accumulation and slow release from most tissues suggests no need for frequent dosing. An initial higher loading dose may be followed by a small periodic “maintenance” dose. However, in attempts to deliver a higher dose to organs like lung, heart and brain, one must bear in mind that very high and possibly toxic levels may be reached in liver, kidneys, and spleen.

Acknowledgement

Ivan Spasojević acknowledges NIH/NCI Duke Comprehensive Cancer Center Core Grant (5-P30-CA14236-29). Ines Batinić-Haberle appreciates financial support from NIH- IR21-ESO/3682, and NIH U19 AI67798-01/pilot project. Yumin Chen, Teresa Noel and Daret St. Clair are thankful to the support of NIH grants CA 49797, CA 73599 and CA 94853. We are thankful to Huaxin Sheng for his help with animal perfusion. Authors are thankful to Irwin Fridovich for critical reading of the manuscript.

Abbreviations

SOD, superoxide dismutase
MnP, Mn^{III}TM-2(3,4)-PyP^{5+}, Mn(III) *meso*-tetrakis{*N*-methylpyridinium-2(3,4)-yl} porphyrin; 2, 3, and 4 being *ortho*, *meta* and *para* isomer, respectively
Mn^{III}TE-2-PyP^{5+}, Mn(III) *meso*-tetrakis(*N*-ethylpyridinium-2-yl)porphyrin (AEOL-10113)
Zn^{II}TE-2-PyP^{4+}, Mn(III) *meso*-tetrakis(*N*-ethylpyridinium-2-yl)porphyrin
MnTnHex-2-PyP^{5+}, Zn *meso*-tetrakis(*N*-n-hexylpyridinium-2-yl)porphyrin
Zn^{II}TnBu-2-PyP^{4+}, Zn *meso*-tetrakis(*N*-n-butylpyridinium-2-yl)porphyrin
H_2Talkyl-2-PyP^{4+}, *meso*-tetrakis(*N*-alkylpyridinium-2-yl)porphyrin *meso* is indicating substitution in 5,10,15,20 positions on porphyrin core
HIF-1, hypoxia inducible factor-1, NF-κB, nuclear factor κB
AP-1, activator protein-1
BSA, bovine serum albumin
TFA, trifluoroacetic acid
PBS, phosphate-buffered saline

References

1. Batinić-Haberle I, Benov L, Spasojević I, Fridovich I. The *Ortho* Effect makes manganese (III) *meso*-tetrakis(*N*-methylpyridinium-2-yl)porphyrin (MnTM-2-PyP) a powerful and potentially useful superoxide dismutase mimic. J. Biol. Chem 1998;273:24521–24528. [PubMed: 9733746]
2. Batinić-Haberle I, Benov L, Spasojević I, Hambright P, Crumbliss AL, Fridovich I. The Relationship Between Redox Potentials, Proton Dissociation Constants of Pyrrolic Nitrogens, and *in Vitro* and *in Vivo* Superoxide Dismutase Activities of Manganese(III) and Iron(III) Cationic and Anionic Porphyrins. Inorg. Chem 1999;38:4011–4022.
3. Batinić-Haberle I, Spasojević I, Stevens RD, Hambright P, Neta P, Okado-Matsumoto A, Fridovich I. New Class of Potent Catalysts of $O_2^{\cdot -}$ Dismutation. Mn(III) methoxyethylpyridyl- and methoxyethylimidazolylporphyrins. J. Chem. Soc. Dalton Trans 2004:1696–1702.
4. Batinić-Haberle I, Spasojević I, Stevens RD, Hambright P, Fridovich I. Manganese(III) *Meso* Tetrakis *Ortho N*-alkylpyridylporphyrins. Synthesis, Characterization and Catalysis of $O_2^{\cdot -}$ Dismutation. J. Chem. Soc., Dalton Trans 2002:2689–2696.
5. Rebouças JS, DeFreitas-Silva G, Idemori YM, Spasojević I, Benov L, Batinić-Haberle I. The impact of electrostatics in redox modulation of oxidative stress by Mn porphyrins. The impact of electrostatics in redox modulation of oxidative stress by Mn porphyrins. Protection of SOD-deficient *E. coli* via alternative mechanism where Mn porphyrin acts as a Mn-carrier. Free Radic. Biol. Med 44
6. Rebouças JS, Spasojević I, Tjahjono DH, Richaud A, Mendez F, Benov L, Batinić-Haberle I. Redox modulation of oxidative stress by Mn porphyrin-based therapeutics: The effect of charge distribution. Dalton Trans 2008:1233–1242. [PubMed: 18283384]
7. Batinić-Haberle I, Spasojević I, Stevens RD, Bondurant B, Okado-Matsumoto A, Fridovich I, Vujasković Z, M Dewhirst WD. New PEG-ylated Mn(III) porphyrins approaching catalytic activity of SOD enzyme. Dalton Trans 2006:617–624. [PubMed: 16402149]
8. Rebouças JS, Spasojević I, Batinić-Haberle I. Pure manganese(III) 5,10,15,20-tetrakis(4- benzoic acid) porphyrin (MnTBAP) is not a superoxide dismutase mimic in aqueous systems: A case of structure-activity relationship as a watchdog mechanism in experimental therapeutics and biology. J. Inorg. Biol. Chem 2008;13:289–302.
9. Lawrence GD, Sawyer DT. Potentiometric titrations and oxidation-reduction potentials of manganese and copper-zinc superoxide dismutases. Biochemistry 1979;18:3045–3050. [PubMed: 380641]
10. Barrette WC Jr, Sawyer DT, Free JA, Asada K. Potentiometric titrations and oxidation-reduction potentials of several iron superoxide dismutases. Biochemistry 1983;22:624–627. [PubMed: 6340720]
11. Ellerby RM, Cabelli DE, Graden JA, Valentine JS. Copper-Zinc Superoxide Dismutase: Why Not pH-Dependent? J. Am. Chem. Soc 1996;118:6556–6561.
12. Vance CK, Miller AF. A Simple Proposal That Can Explain the Inactivity of Metal-Substituted Superoxide Dismutases. J. Am. Chem. Soc 1998;120:461–467.
13. Michel E, Nauser T, Sutter B, Bounds PL, Koppenol WH. Kinetics properties of Cu,Zn-superoxide dismutase as a function of metal content. Arch. Biochem. Biophys 2005;439:234–240. [PubMed: 15978540]
14. Goldstein S, Fridovich I, Czapski G. Kinetic properties of Cu,Zn-superoxide dismutase as a function of metal content –Order restored. Free Radic. Biol. Med 2006;41:937–941. [PubMed: 16934676]
15. Ferrer-Sueta G, Vitturi D, Batinić-Haberle I, Fridovich I, Goldstein S, Czapski G, Radi R. Reactions of Manganese Porphyrins with Peroxynitrite and Carbonate Radical Anion. J. Biol. Chem 2003;278:27432–27438. [PubMed: 12700236]
16. Ferrer-Sueta G, Batinić-Haberle I, Spasojević I, Fridovich I. Peroxynitrite Scavenging by Manganese (III) Meso-Tetrakis-(*N*-methylpyridyl)Porphyrins. Chem. Res. Toxicol 1999;12:442–449. [PubMed: 10328755]
17. Ferrer-Sueta G, Hannibal L, Batinić-Haberle I, Radi R. Reduction of manganese porphyrins by flavoenzymes and submitochondrial particles and the catalytic redox cycle of peroxynitrite. Free Radic. Biol. Med 2006;41:503–512. [PubMed: 16843831]
18. Rahamn I, Adcock IM. Oxidative stress and redox regulation of lung inflammation in COPD. Eur. J. Resp 2006;28:219–242.

19. Van Empel VPM, Bertrand AT, Van Oort RJ, Van der Nagel R, Engelen M, Van Rijen HV, Doevendans PA, Crijns HJ, Ackerman SL, Sluiter W, De Windt LJ. EUK-8, a superoxide dismutase and catalase mimetic reduces cardiac oxidative stress and ameliorates pressure overload-induced heart failure in the Harlequin mouse mutant. J. Amer. Coll. Cardiol 2006;48:824–832. [PubMed: 16904556]
20. Cuzzocrea S, Pisano B, Dugo L, Ianartao A, Ndenglele M, Salvemini D. Superoxide-related signaling cascade mediates nuclear factor-κB activation in acute inflammation. Antiox. Redox Signal 2004;6:699–704.
21. Floyd RA. Nitrones as therapeutics in age-related diseases. Aging Cell 2006;5:51–57. [PubMed: 16441843]
22. Xu Y, Kalyanaraman B. Synthesis and ESR studies of a novel cyclic nitrone spin trap attached to a phosphonium group -a suitable trap for mitochondria-generated ROS. Free Radic Res 2007;41:1–7. [PubMed: 17164173]
23. Soule BP, Hyodo F, Matsumoto K, Simone NL, Cook JA, Krishan MC, Mitchell JB. The chemistry and biology of nitroxides. Free Radic. Biol. Med 2007;42:1632–1650. [PubMed: 17462532]
24. Murphy MP, Smith RAJ. Targeting antioxidants to mitochondria by conjugation to lipophilic cations. Annu. Rev. Pharmacol. Toxicol 2007;47:629–656. [PubMed: 17014364]
25. Dhanasekaran A, Kotamraju S, Kalivendi SV, Matsunaga T, Shang T, Keszler A, Joseph J, Kalyanaraman B. Supplementation of endothelial cells with mitochondria-targeted antioxidants inhibit peroxide-induced mitochondrial iron uptake, oxidative damage, and apoptosis. J. Biol. Chem 2004;279:37575–37587. [PubMed: 15220329]
26. Zhao Y, Chaiswing L, Oberley TD, Batinić-Haberle I, St. Clair W, Epstein CJ, St. Clair D. A mechanism-based antioxidant approach for the reduction of skin carcinogenesis. Cancer Res 2005;65:1401–1405. [PubMed: 15735027]
27. Zhao Y, Chaiswing L, Velez JM, Batinić-Haberle I, Colburn NH, Oberley TD, St. Clair DK. p53 translocation to mitochondria precedes its nuclear translocation and targets mitochondrial oxidative defense protein-manganese superoxide dismutase. Cancer Res 2005;65:3745–3750. [PubMed: 15867370]
28. Moeller BJ, Batinić-Haberle I, Spasojević I, Rabbani ZN, Anscher MS, Vujasković Z, Dewhirst MW. Effects of a catalytic metalloporphyrin antioxidant on tumor radioresponsiveness. Int. J. Rad. Oncol. Biol. Phys 2005;63:545–552.
29. Moeller BJ, Cao Y, Li CY, Dewhirst MW. Radiation activates HIF-1 to regulate vascular radiosensitivity in tumors: Role of oxygenation, free radicals and stress granules. Cancer Cell 2004;5:429–441. [PubMed: 15144951]
30. Jackson IL, Batinić-Haberle I, Vujasković Z. Superoxide dismutase mimic reduces hypoxia induced-$O_2^{\cdot -}$, TGF-β and VEGF production by macrophages. Free Radic. Res 2007;41:8–14. [PubMed: 17164174]
31. Jackson IL, Batinić-Haberle I, Sonveaux P, Dewhirst MW, Vujasković Z. Superoxide production and angiogenic regulation by macrophages in response to heat. Int. J. Hypothermia 2006;22:263–273.
32. Tse H, Milton MJ, Piganelli JD. Mechanistic analysis of the immunomodulatory effects of a catalytic antioxidant on antigen-presenting cells: Implication for their use in targeting oxidation/reduction reactions in innate immunity. Free Radic Biol Med 2004;36:233–247. [PubMed: 14744635]
33. Bottino R, Balamurugan AN, Tse H, Thirunavukkarasu C, Ge X, Profozich J, Milton M, Ziegenfuss A, Trucco M, Piganelli JD. Response of human islets to isolation stress and the effect of antioxidant treatment. Diabetes 2004;53:2559–2568. [PubMed: 15448084]
34. Spasojević I, Batinić-Haberle I, Rebouças JS, Idemori YM, Fridovich I. Electrostatic Contribution in the Catalysis of $O_2^{\cdot -}$ Dismutation by Superoxide Dismutase Mimics. J. Biol. Chem 2003;278:6831–6837. [PubMed: 12475974]
35. Tauskela JS, Brunette E, Hewitt M, Mealing G, Morley P. Competing approaches to excitotoxic neuro protection by inert and catalytic antioxidant porphyrins. Neurosci. Lett 2006;401:236–241. [PubMed: 16631306]
36. Szabó C, Ischiropoulos H, Radi R. Peroxynitrite: biochemistry, pathophysiology and development of therapeutics. Nature Rev. Drug Discov 2007;6:662–680. [PubMed: 17667957]

37. Szabó C, Mabley JG, Moeller SM, Shimanovich R, Pacher P, Virag L, Soriano VG, van Duzer JH, Williams W, Salzman AL, Groves JT. Part I: pathogenetic role of peroxynitrite in the development of diabetes and diabetic vascular complications: studies with FP15, a novel potent peroxynitrite decomposition catalyst. Mol. Med 2002;8:571–580. [PubMed: 12477967]
38. Pieper GM, Nilakantan V, Chen M, Zhou J, Khanna AK, Henderson JD Jr, Johnson CP, Roza AM, Szabó C. Protective mechanisms of a metalloporphyrinic peroxynitrite decomposition catalyst, WW85, in rat cardiac transplants. J. Pharmacol. Exp. Ther 2005;314:53–60. [PubMed: 15784653]
39. Aviv I, Gross Z. Corrole-based applications. Chem. Commun 2007:1987–1999.
40. Warner DS, Sheng H, Batinić-Haberle I. Oxidants, Antioxidants, and the Ischemic Brain. J. Exp. Biology 2004;207:3221–3231.
41. Sheng H, Enghild J, Bowler R, Patel M, Calvi CL, Batinić-Haberle I, Day BJ, Pearlstein RD, Crapo JD, Warner DS. Effects of Metalloporphyrin Catalytic Antioxidants in Experimental Brain Ischemia. Free. Radic. Biol. Med 2002;33:947–961. [PubMed: 12361805]
42. Mackensen GB, Patel M, Sheng H, Calvi CL, Batinić-Haberle I, Day BJ, Liang LP, Fridovich I, Crapo JD, Pearlstein RD, Warner DS. Neuroprotection from Delayed Post-Ischemic Administration of a Metalloporphyrin Catalytic Antioxidant in the Rat. J. Neurosci 2001;21:4582–4592. [PubMed: 11425886]
43. Sheng H, Spasojević I, Warner DS, Batinić-Haberle I. Mouse spinal cord compression injury is ameliorated by intrathecal manganese(III) porphyrin. Neurosci. Lett 2004;366:220–225. [PubMed: 15276251]
44. Crow JP, Clingasan NY, Chen J, Hill JL, Beal MF. Manganese porphyrin given at symptom onset markedly extends survival of ALS mice. Ann. Neurol. 2005 2005;58:258–265.
45. Sompol P, Ittarat W, Tangpong J, Chen Y, Doubinskaia I, Mohammad Abdul H, Butterfield A, St. Clair DK. A neuronal model of Alzheimer's disease: An insight into the mechanisms of oxidative stress-mediated mitochondrial injury. Neuroscience 2008;153:120–130. [PubMed: 18353561]
46. Rabbani, ZN.; Vasquez-Vivar, J.; Spasojevic, I.; Whitsett, J.; Selvakumar, B.; Haberle, S.; Vujaskovic, Z.; Dewhirst, MW.; Batinic-Haberle, I. Anti-tumor effects of Mn(III) ortho tetrakis *N*-ethylpyridylporphyrin, MnTE-2-PyP^{5+} in mice model of breast tumor. San Diego: AACR; 2008.
47. Rabbani Z, Salahuddin FK, Yarmolenko P, Batinić-Haberle I, Trasher BA, Gauter-Fleckenstein B, Dewhirst MW, Anscher MS, Vujasković Z. Low molecular weight catalytic metalloporphyrin antioxidant AEOL10150 (5 mg/kg) protects rat lungs from chronic radiation-induced injury. Free Radic. Res 2007;41:1273–1282. [PubMed: 17957541]
48. Gauter-Fleckenstein B, Fleckenstein K, Owzar K, Jian C, Batinić-Haberle I, Vujasković Z. Comparison of two Mn porphyrin-based mimics of superoxide-dismutase (SOD) in pulmonary radioprotection. Free Radic Biol Med 2008;44:982–989. [PubMed: 18082148]
49. Rabbani Z, Batinić-Haberle I, Anscher MS, Huang J, Day BJ, Alexander E, Dewhirst MW, Vujasković Z. Long term administration of a small molecular weight catalytic metalloporphyrin antioxidant AEOL10150 protects lungs from radiation-induced injury. Int. J. Rad. Oncol. Biol. Phys 2007;67:573–580.
50. Piganelli JD, Flores SC, Cruz C, Koepp J, Young R, Bradley B, Kachadourian R, Batinić-Haberle I, Haskins K. A Metalloporphyrin Superoxide Dismutase Mimetic (SOD Mimetic) Inhibits Autoimune Diabetes. Diabetes 2002;51:347–355. [PubMed: 11812741]
51. Benov L, Batinić-Haberle I. A manganese porphyrin SOD mimic suppresses oxidative stress and extends the life span of streptozotocin-diabetic rats. Free Radic. Res 2005;38:81–88. [PubMed: 15875815]
52. Aslan M, Ryan TM, Adler B, Townes TM, Parks DA, Thompson JA, Tousson A, Gladwin MT, Tarpey MM, Patel RP, Batinić-Haberle I, White CR, Freeman BA. Oxygen Radical Inhibition of Nitric-Oxide Dependent Vascular Function in Sickle Cell Disease. Proc. Natl. Acad. Sci. USA 2001;98:15215–15220. [PubMed: 11752464]
53. Csont T, Viappiani S, Sawicka J, Slee S, Altarejos JY, Batinić-Haberle I, Schulz R. The Involvement of Superoxide and iNOS-Derived NO in Cardiac Dysfunction Induced by Pro-Inflammatory Cytokines. J. Mol. Cell. Card 2005;39:833–840.

54. Saba H, Batinić-Haberle I, Munusamy S, Mitchell T, Lichti C, Megyesi J, MacMillan-Crow LA. Manganese porphyrin reduces renal injury and mitochondrial damage during ischemia/reperfusion. Free Radic. Biol. Med 2007;42:1571–1578. [PubMed: 17448904]
55. Wu TJ, Khoo NH, Zhou F, Day BJ, Parks DA. Decreased hepatic ischemia-reperfusion injury by manganese-porphyrin complexes. Free Radic Res 2007;41:127–134. [PubMed: 17364938]
56. Cernanec JM, Weinberg BJ, Batinić-Haberle I, Guilak F, Fermor B. Oxygen tension modulates the effects of interleukin-1 on articular cartlidge matrix turnover via peroxynitrite. J. Rheumatol 2007;34:401–407. [PubMed: 17295437]
57. Spasojević I, Yumin C, Noel T, Yu I, Pole MP, Zhang L, Zhao Y, St. Clair DK, Batinić-Haberle I. Mn porphyrin-based SOD mimic, MnTE-2-PyP^{5+} targets mouse heart mitochondria. Free Radic. Biol. Med 2007;42:1193–1200. [PubMed: 17382200]
58. Spasojević I, Menzeleev R, White PS, Fridovich I. Rotational Isomers of *N*-alkylpyridylporphyrins and their Metal Complexes. HPLC Separation, ^{1}H NMR and X-ray Structural Characterization, Electrochemistry and Catalysis of $O_2^{\cdot -}$ Disproportionation. Inorg. Chem 2002;41:5874–5881. [PubMed: 12401096]
59. Benov L, Batinić-Haberle I, Spasojević I, Fridovich I. Isomeric *N*-alkylpyridylporphyrins and their Zn(II) Complexes: Inactive as SOD Mimics but are Powerful Photosenzitizers. Arch. Biochem. Biophys 2002;402:159–165. [PubMed: 12051659]
60. Kalyanasundaram K. Photochemistry of water-soluble porphyrins: Comparative study of isomeric tetrapyridyl- and tetrakis(N-methylpyridiniumyl)porphyrins. Inorg. Chem 1984;23:2453–2459.
61. Vergeldt FJ, Koehorst RBM, Van Hoek A, Schaafsma TJ. Intramolecular interactions in the ground and excited state of tetrakis(N-methylpyridyl)porphyrins. J. Phys. Chem 1995;99:4397–4405.
62. Quimby DJ, Longo FR. Luminescence studies of several tetrarylporphyrins and their Zn derivatives. J. Am. Chem. Soc 1975;97:5111–5117.
63. Batinić-Haberle I, Ndengle MM, Cuzzocrea S, Rebouças JS, Matuschak GM, St. Clair DK, Dewhirst MW, Spasojević I, Salvemini D. Inhibition of morphine antinociceptive tolerance and suppression of tumor angiogenesis: Dual action of Mn porphyrin-based drugs in cancer therapy and pain management. AACR. 2008
64. Vujaskovic Z, Batinic-Haberle I, Rabbani ZN, Feng Q-F, Kang SK, Spasojevic I, Samulski TV, Fridovich I, Dewhirst MW, Anscher MS. A Small Molecular Weight Catalytic Metalloporphyrin Antioxidant with Superoxide Dismutase (SOD) Mimetic Properties Protects Lungs from Radiation-Induced Injury. Free. Radic. Biol. Med 2002;33:857–863. [PubMed: 12208373]
65. Spasojevic I, Colvin OM, Warshany KR, Batinic-Haberle I. New approach to the activation of anti-cancer pro-drug by metallporphyrin-based cytochrome P450 mimics in all-aqueous biologically relevant system. J. Inorg. Biochem 2006;100:1897–1902. [PubMed: 16965820]
66. Day B, Kariya C. A novel class of cytochrome P450 reductase redox cyclers: Cationic manganoporphyrins. Toxicol. Sci 2005;85:713–719. [PubMed: 15703263]
67. Bansal S, DeStefano A. Key elements of bioanalytical method validation for small molecules. AAPS J 2007;9:E109–E114. [PubMed: 17408234]
68. Muscoli C, Cuzzocrea S, Ndengele MM, Mollace V, Porreca F, Fabrizi F, Espositio E, Masini E, Matuschak GM, Salvemini D. Therapeutic manipulation of peroxynitrite attenuates the development of opiate-induced antinociceptive tolerance in mice. J. Clin. Invest 2007;117:3185–3539. [PubMed: 17975665]
69. Okado-Matsumoto A, Batinic-Haberle I, Fridovich I. Complementation of SOD deficient *Escherichia* coli by manganese porphyrin mimics of superoxide dismutase. Free Radic. Biol. Med 2004;37:401–410. [PubMed: 15223074]
70. Vinnakota KC, Bassingthwaighte JB. Myocardial density and composition: a basis for calculating intracellular metabolite concentrations. Am. J. Physiol. Heart Circ. Physiol 2004;286:H1742–H1749. [PubMed: 14693681]

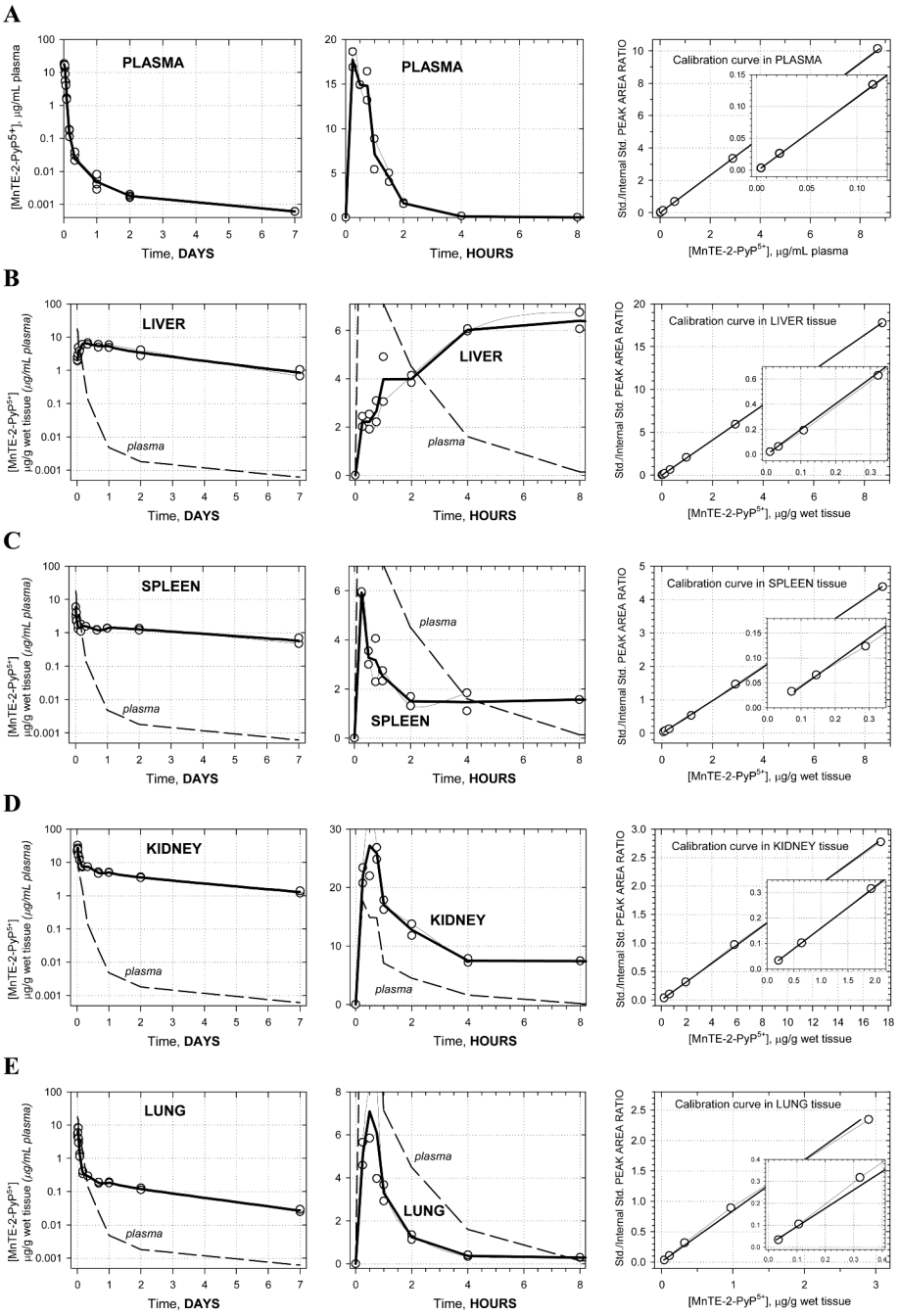

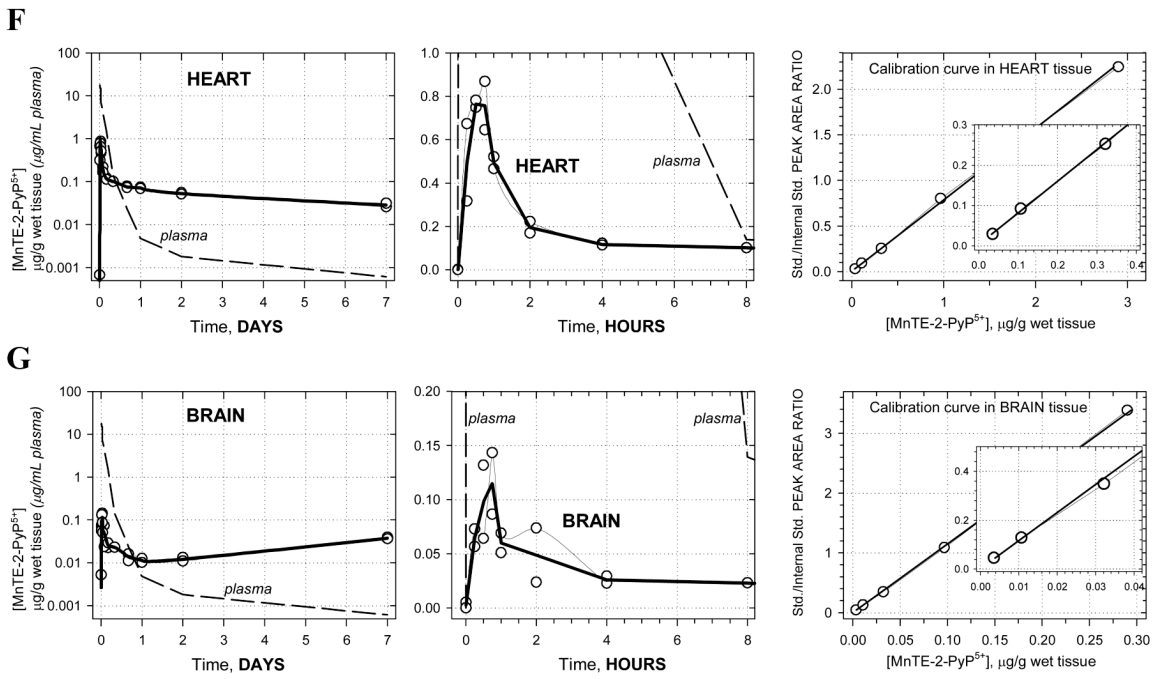

Figure 1.

Pharmacokinetics of MnTE-2-PyP^{5+} in plasma (A), liver (B), spleen (C), kidney (D), lung (E), heart (F) and brain (G). Levels of porphyrin are given in μg per mL of plasma or per g of wet tissue. Drug was given at a single intraperitoneal dose of 10 mg/kg to female B6C3F1 mice. Animals were anesthesized, perfused and organs excised. 2 mice were used per data point. Calibration curves were done in plasma and related organs. The known amounts of MnTE-2-PyP^{5+} were added into the plasma and organ homogenates; the rest of the procedure was identical to the one used for drug-treated mice.

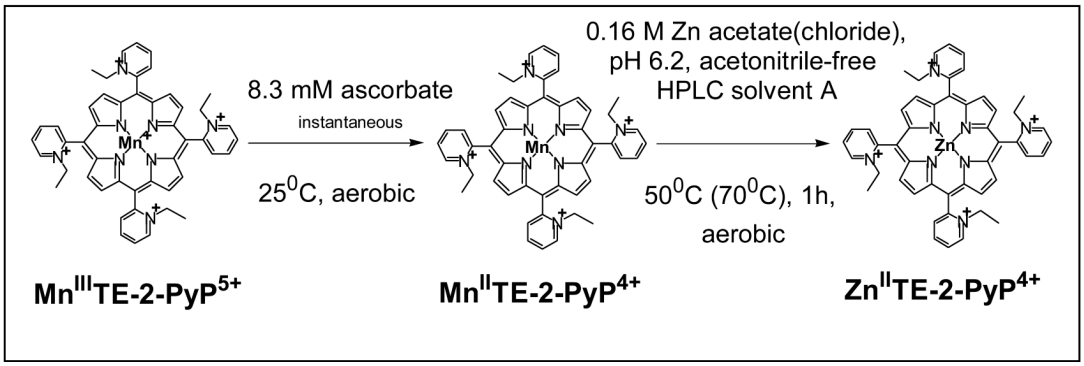

Scheme I.

The representation of the method used to determine levels of MnTE-2-PyP^{5+} in plasma and organs. After the proteins were precipitated from plasma and tissue homogenates, the Zn salt was added along with sodium ascorbate into the supernatant to exchange Mn(II) by Zn(II). While the reduction of the Mn(III)P occurred instantaneously, one hour of incubation at 50 or 70 °C is needed to yield a complete Mn by Zn exchange for the HPLC/fluorescence measurement of ZnTE-2-PyP^{4+}.

Table 1

Pharmacokinetic parameters of MnTE-2-PyP^{5+} in plasma, liver, kidney, spleen, lung, heart and brain: t_{max} (time point where maximum concentration, c_{max} was achieved), c_{max} (maximum observed concentration), $t_{1/2}$ (half life of MnTE-2-PyP^{5+} elimination obtained from terminal slope between days 2 and 7), AUC_{last} (area under the curve up to the last measurement, i.e. 7 days) and AUC_{inf} (projected total area under the curve at infinite time point) that indicates the exposure of the organ to the drug.

organ	t_{max}, h	c_{max}, μg/g	$t_{1/2}$,h	AUC_{last}, μg · h/mL(g)	AUC_{inf}, μg · h/mL(g)
plasma	0.25	17.74	76.9	18.7	18.8
liver	8	6.40	60.1	459.1	533.7
spleen	0.25	5.92	107.0	174.5	265.2
kidney	0.5	27.17	82.0	543.4	695.8
lung	0.75	0.12	55.5	24.4	26.5
heart	0.5	0.76	135.0	9.2	14.8
brain	0.75	0.11 (0.04)*	-**	3.6	-**

Clearance (= dose/AUC) of the drug from body was calculated from plasma data to be 0.53 mg/kg/h.

* value at 7-day time point ($C_{max[LAST]}$)

** no terminal phase achieved